

Diagenetic Model for the Deep Montney Formation, Northeastern British Columbia

N. Vaisblat, University of Alberta, Edmonton, AB, vaisblat@ualberta.ca

N.B. Harris, University of Alberta, Edmonton, AB

C. DeBhur, University of Calgary, Calgary, AB

T. Euzen, IFP Technologies Inc., Calgary, AB

M. Gasparrini, IFP Energies nouvelles, Rueil-Malmaison, France

V. Crombez, IFP Energies nouvelles, Rueil-Malmaison, France

S. Rohais, IFP Energies nouvelles, Rueil-Malmaison, France

F. Krause, University of Calgary, Calgary, AB

K. Ayranci, University of Alberta, Edmonton, AB

Vaisblat, N., Harris, N.B., DeBhur, C., Euzen, T., Gasparrini, M., Crombez, V., Rohais, S., Krause, F. and Ayranci, K. (2017): Diagenetic model for the deep Montney Formation, northeastern British Columbia; *in* Geoscience BC Summary of Activities 2016, Geoscience BC, Report 2017-1, p. 37–48.

Introduction

The Lower Triassic Montney Formation of the Western Canada Sedimentary Basin (WCSB) is a world-class unconventional resource with 450 Tcf gas reserves, 14 520 mmbbl natural gas liquids reserves and 1125 mmbbl oil reserves (National Energy Board, 2013). Although commonly described as a shale, the Montney Formation is a siltstone in most of its subcrop. Unlike sandstone and shale reservoirs, little is known about the diagenetic evolution and pore development of siltstone reservoirs, and a better understanding of diagenetic controls on reservoir quality in this type of reservoir is essential to improve resource and reserve estimates and to maximize hydrocarbon recovery. This work focuses on the deepest section of the Montney Formation in British Columbia (BC). An isopach map of the formation thickness and the location of the study area are presented in Figure 1. In this area, the Montney Formation is within the gas window and highly mature (temperature at maximum release of hydrocarbons [T_{\max}] is $>470^{\circ}\text{C}$, vitrinite reflectance [R_o] is 1.3%).

Diagenetic studies are crucial for understanding pore system evolution and predicting reservoir quality. The objective of this paper is to describe the major authigenic phases that are present in the Montney Formation siltstone and in-

terpret the temporal sequence of events leading to the consolidation of the formation.

Geological Background

The Montney Formation is a west-dipping clastic wedge, deposited on the western continental shelf of Pangea. The Montney Formation consists of three third-order sequences prograding from east to west. In the western part of the basin, the Montney Formation is topped by a major intra-Triassic erosive surface and overlain by the transgressive Doig Formation (Crombez, 2016). The formation reaches a maximum thickness of 350 m adjacent to the Rocky Mountains deformation front, and thins eastward to an erosional zero edge in the east (Figure 1). The centre of the Montney Formation depositional basin was positioned at a paleolatitude of approximately 30°N (Golonka et al., 1994; Davies et al., 1997; Deep Times Maps Inc.TM, 2013), experiencing a semi-arid to desert climate (Gibson and Barclay, 1989; Davis et al., 1997), and dominated by west winds (Edwards et al., 1994; Golonka et al., 1994).

Grain sizes in the Montney Formation range from silt to very fine sand, with grains typically moderately to well sorted, and subrounded to rounded (Davies et al., 1997; Barber, 2003). Sorting and roundness indicate a predominantly aeolian transport mechanism with periodic fluvial influence (Davies et al., 1997; Barber, 2003; Moslow and Zonneveld, 2012). The mineralogy of the Montney Formation (high in feldspar and detrital dolomite) supports the interpretations of an arid climate and suggests a depositional model of wind-blown, recycled immature material originating from the quartz-rich shield in the east (Edwards et al., 1994; Davies et al., 1997; Barber, 2003; Moslow and

Keywords: *British Columbia, Montney Formation, diagenesis, paragenesis, quartz cement, dolomite cement, dissolution, reservoir quality, clay minerals*

This publication is also available, free of charge, as colour digital files in Adobe Acrobat[®] PDF format from the Geoscience BC website: <http://www.geosciencebc.com/s/DataReleases.asp>.

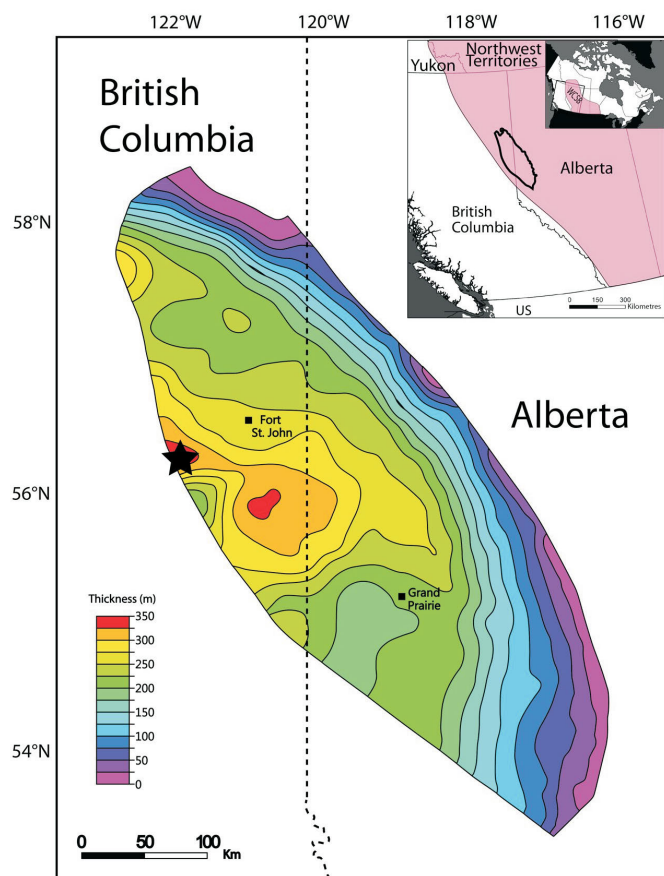


Figure 1. Isopach map of the thickness of the Montney Formation (modified from Edwards et al., 1994) and its location within the Western Canada Sedimentary Basin (WCSB). Study area is marked by the black star.

Zonneveld, 2012). Deposition of the Montney Formation took place in an anoxic to dysoxic environment, with several periods of higher oxygen levels evidenced by bioturbated intervals (Robbins, 1999; Nassichuk, 2000; LaMothe, 2008; Zonneveld et al., 2010a, b, 2011; Moslow and Zonneveld, 2012; Playter, 2013; Crombez, 2016; Crombez et al., 2016).

Previous Work

Few diagenetic studies have been conducted on the Montney Formation. Davies et al. (1997) and Barber (2003) studied diagenesis in the Montney Formation of west-central Alberta (Sturgeon Lake South ‘F’ pool), and Nassichuk (2000), Chalmers and Bustin (2012) and Playter (2013) investigated the diagenetic sequences of the Montney Formation in northeastern BC. Investigation methods vary between studies, and paragenetic interpretations are inconsistent. The major diagenetic phases described are calcite, dolomite, feldspar and quartz cements. Pyrite is reported to be widely present throughout the Montney Formation. Authigenic clays identified are fibrous illite, chlorite and glauconite, and diagenetic illitization of smectite.

Secondary porosity resulted from grain dissolution (aragonite, calcite, feldspar and quartz) or dedolomitization (Playter, 2013). Carbonate cementation is usually described as the earliest pore-occluding event, followed by quartz cement. Pyrite precipitation is thought to have occurred more or less continuously (Davies et al., 1997; Playter, 2013). Authigenic clay precipitation occurred in an intermediate stage, followed by quartz and feldspar dissolution and a second phase of carbonate (calcite and/or dolomite) precipitation. Ducros et al. (2014) estimated 2200 m of erosion above the Montney Formation in the research area during the Laramide orogeny, bringing the Montney Formation to a maximum burial depth of approximately 4700 m. The modelled maximum temperature for the Montney Formation at maximum burial depth is 180°C (Vaisblat and Harris, 2016).

Dataset

The majority of the samples for this study were selected from the Progress et al. Altares 16-17-083-25 wellcore (universal well identifier 100161708325W600, BC Oil and Gas Commission, 2016), which represents the entire section of the Montney Formation at its thickest location in the basin (sequences 1, 2 and 3 of Crombez et al. [2016], equivalent to the lower and upper Montney Formation). Sixty-eight samples were taken from this core between 2258 and 2530 m. Fifteen additional samples were made available for this study from the Suncor PC HZ Kobes D-048-B/094-B-09 wellcore (universal well identifier 200D048A094B0900, 200B079A094B0902), representing Spathian age strata (Golding et al., 2015).

Those samples were the focus of the work done by Playter (2013). Both wells are situated in the study area (Figure 1).

Methods

Since grain size in the Montney Formation, particularly in the deep section, is very fine, standard thin section analysis has proven ineffective for detailed diagenetic study. For this reason, all analyses were carried out using a scanning electron microscope (SEM).

Rock Composition

Samples were cut perpendicular to bedding, mounted in epoxy and polished to expose a surface of approximately 1.5 cm². Inorganic rock composition of these samples was determined by QEMSCAN[®] (Quantitative Evaluation of Minerals by SCANNing electron microscopy) at SGS Canada Inc. (Vancouver, BC). The QEMSCAN method is based on an FEI Company Quanta 650 with multiple energy dispersive spectrometry (EDS) detectors. Mineral identification was made by matching the spectral response with a proprietary species identification protocol (SIP), a comprehensive mineral library, which includes reference composi-

tions and solid solution series. The composition of three randomly selected samples was also determined by quantitative X-ray diffraction (XRD) analysis on a homogenized sample, representing approximately 10 cm of core. Clay minerals expandability potential was determined using oriented, glycolated mounts of the <2 µm fraction. Analysis was done at the James Hutton Institute (Aberdeen, Scotland). Whole rock X-ray powder diffraction patterns were recorded from 3–70° 2θ, and clay mounts were recorded from 3–45° 2θ, using copper Kα radiation. Organic rock composition, also performed on ~10 cm homogenized sample, was obtained by LECO TOC (total organic carbon) analysis at GeoMark Research, Ltd. laboratories (Houston, Texas).

Diagenetic Phases

Both freshly broken surfaces and polished surfaces were examined in order to identify the diagenetic phases present in the rock. Some of the samples were coated with gold and examined on a JEOL Ltd. 6301F field emission SEM (FE-SEM) with an accelerating voltage of 20 kilovolts (kV) at the University of Alberta (Edmonton, Alberta). Other samples were coated with carbon and examined on a Zeiss EVO LS15 extended pressure SEM (EP-SEM) with an accelerating voltage of 20 kV, also at the University of Alberta. Elemental content was determined using an energy dispersive X-ray analyzer attached to the SEM.

Selected samples were polished with an E.A. Fischione Instruments, Inc. 1060 SEM mill at 5 kV, 3° and continuous rotation for three hours. Samples were examined on an FEI Company Quanta 250 FEG with a Gatan, Inc. MonoCL4™ detector (SEM-CL) at the University of Calgary (Calgary, Alberta). For each sample, three or four areas were randomly selected and analyzed for mineralogical composition and luminescence patterns. Image analysis was con-

ducted to differentiate mineralogical and diagenetic phases for each mineral.

Results and Morphological Observations

Since the two well locations examined in this study are <40 km apart, results will be presented for both cores together.

Minerals present in the rock include quartz, feldspar, plagioclase, carbonate minerals, pyrite, apatite, muscovite, chlorite, mixed-layered illite-smectite (MLIS) and kaolinite, and minor amounts of other sulphides and heavy minerals (Table 1). Total organic carbon values in the samples range between 0.5 and 4 wt. % with an average of 1.5 wt. %. Organic matter in the formation displays a wide spectrum of morphologies from nonporous to extremely porous. This phenomenon was previously recognized in shales, and attributed by Curtis et al. (2011) to differences in organic matter composition.

Diagenetic Processes

Diagenetic processes were interpreted through a combination of compositional analysis, SEM-imaging observations and cathodoluminescence image interpretation.

Porosity Occluding Processes

Compaction

Physical compaction followed by chemical compaction is evidenced in all samples by pressure solutions of framework grains, mainly quartz, feldspars and dolomite (Figure 2).

Dolomite

Dolomite in the deep Montney Formation varies in origin and composition. Detrital dolomite, evidenced by weathered rounded cores, is surrounded by rhombs of authigenic dolomite cement. Small rhombohedral dolomite crystals do not always contain a detrital core. At least seven genera-

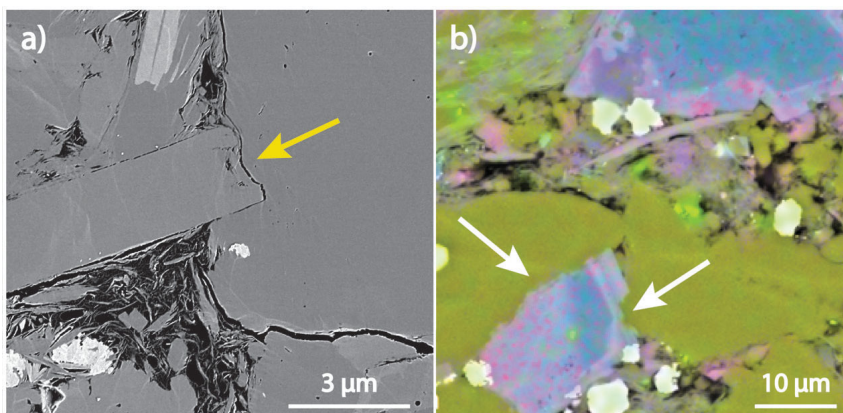


Figure 2. Evidence for chemical compaction in Montney Formation, northeastern British Columbia: **a)** backscattered electron (BSE) image of mica penetrating a quartz grain and **b)** energy dispersive spectrometry (EDS) image of quartz grain (greenish-yellow) dissolving dolomite (light blue) with authigenic rims.

Table 1. Mineralogical composition (%) and total organic carbon (wt. %) for samples from the Progress et al. Altares 16-17-083-25 wellcore (universal well identifier 100161708325W600, BC Oil and Gas Commission, 2016) were obtained by QEMSCAN® analysis.

Depth ¹	TOC	Quartz	K-feldspar	Plagioclase	Muscovite	Biotite	Kaolinite	Chlorite	Illite/ MLIS	Calcite	Dolomite	Fe- dolomite	Fe oxide and siderite	Pyrite	Sulphides ²	Fluorite	Ti silicates	Apatite	Heavy minerals
2260	0.98	36.66	9.59	7.44	2.40	0.08	0.40	0.20	6.48	6.95	22.09	0.01	0.00	4.17	0.32	0.01	0.40	1.74	0.08
2265	--	38.40	11.03	10.10	4.19	0.08	0.40	0.16	10.10	8.80	11.51	0.01	0.00	3.91	0.21	0.02	0.45	0.50	0.12
2268	2.21	37.04	9.86	9.11	2.97	0.09	0.41	0.17	8.27	9.72	14.13	0.03	0.00	4.66	0.32	0.02	0.42	0.49	0.08
2273	--	35.91	10.18	8.85	3.80	0.11	0.44	0.16	10.90	9.82	14.70	0.07	0.00	3.94	0.23	0.01	0.40	0.43	0.06
2275	1.30	30.94	9.06	6.81	4.26	0.17	0.67	0.16	13.68	5.97	22.32	0.40	0.00	3.14	0.22	0.01	0.36	0.47	0.07
2278	--	31.88	9.06	7.66	3.44	0.13	0.50	0.18	11.18	10.86	17.13	3.30	0.00	3.56	0.24	0.01	0.40	0.42	0.06
2282	3.25	35.25	10.16	8.27	3.48	0.08	0.41	0.12	10.67	12.36	10.65	1.47	0.00	2.50	0.40	0.02	0.41	0.40	0.09
2286	--	34.39	10.76	8.33	4.71	0.13	0.53	0.16	14.43	9.14	11.52	1.97	0.00	2.60	0.28	0.02	0.44	0.54	0.07
2290	3.14	34.30	9.91	8.43	3.85	0.09	0.46	0.14	12.85	11.97	10.03	1.43	0.00	2.30	0.24	0.03	0.39	0.37	0.07
2293	--	36.63	8.87	8.49	3.08	0.17	0.58	0.26	8.93	6.97	18.90	4.20	0.01	1.76	0.15	0.01	0.40	0.51	0.09
2299	1.03	34.38	8.87	8.84	3.59	0.11	0.45	0.28	8.00	6.85	14.50	10.47	0.04	1.37	0.11	0.02	0.38	0.36	0.06
2301	--	35.30	8.88	9.58	4.53	0.16	0.60	0.31	10.27	3.83	16.86	6.77	0.03	1.74	0.18	0.01	0.43	0.43	0.08
2306	1.30	38.26	11.21	11.38	4.94	0.09	0.39	0.18	12.17	5.52	7.76	3.72	0.02	2.03	0.15	0.01	0.44	0.36	0.08
2308	--	37.70	10.99	11.44	5.69	0.12	0.50	0.26	11.36	3.31	11.19	4.25	0.02	1.97	0.22	0.01	0.43	0.44	0.08
2310	2.21	33.40	10.92	9.83	6.40	0.14	0.51	0.20	16.70	2.30	10.93	2.89	0.01	2.56	0.19	0.00	0.41	0.37	0.05
2324	--	18.11	3.10	3.91	2.09	0.17	0.69	0.37	4.69	3.32	35.08	26.67	0.20	1.08	0.07	0.01	0.21	0.20	0.03
2328	1.81	37.88	8.25	9.38	4.05	0.12	0.58	0.24	11.94	5.35	13.10	3.75	0.17	2.05	0.21	0.01	0.39	0.64	0.08
2332	--	25.21	5.46	5.82	2.43	0.22	0.64	0.39	8.45	2.62	28.26	17.31	0.07	2.34	0.12	0.01	0.28	0.31	0.04
2334	1.00	37.66	10.59	11.01	5.71	0.12	0.47	0.23	13.74	3.37	9.34	3.53	0.08	2.10	0.21	0.01	0.39	0.36	0.08
2338	--	36.26	11.21	10.56	5.57	0.13	0.52	0.23	13.69	4.82	10.86	3.23	0.19	1.75	0.16	0.01	0.39	0.34	0.09
2343	0.82	38.60	8.53	10.43	4.68	0.09	0.50	0.25	10.24	6.71	10.27	5.12	0.42	2.05	0.32	0.02	0.45	0.41	0.09
2346	0.90	37.55	8.90	11.31	5.82	0.09	0.56	0.23	11.65	6.54	9.05	4.25	0.25	1.84	0.24	0.01	0.40	0.32	0.09
2350	--	39.74	8.66	10.91	4.53	0.08	0.51	0.26	9.11	7.42	9.62	5.51	0.49	1.95	0.21	0.02	0.41	0.44	0.13
2354	1.02	34.27	8.15	10.07	7.42	0.11	0.66	0.28	14.21	5.12	9.10	5.68	0.43	2.30	0.21	0.01	0.40	0.49	0.07
2356	1.90	34.95	8.26	9.43	6.87	0.11	0.62	0.20	15.78	6.88	8.60	2.26	0.62	2.50	0.24	0.02	0.36	0.33	0.07
2360	--	27.93	7.11	7.12	4.05	0.15	0.67	0.33	11.07	4.88	22.68	10.18	0.13	2.90	0.16	0.01	0.30	0.26	0.06
2364	2.68	35.85	8.58	9.69	6.12	0.13	0.62	0.22	16.02	5.36	9.33	2.22	0.16	1.98	0.19	0.01	0.37	0.38	0.09
2368	--	28.48	9.47	6.00	3.82	0.13	0.50	0.15	16.45	7.33	10.60	2.03	0.13	1.76	0.19	0.01	0.24	12.67	0.04
2372	1.95	37.46	11.50	11.21	5.32	0.11	0.47	0.22	13.08	4.15	8.37	1.87	0.02	3.17	0.22	0.00	0.47	0.35	0.07
2376	--	38.25	11.06	11.40	3.76	0.21	0.32	0.30	15.61	5.22	4.54	2.58	0.01	5.61	0.27	0.00	0.51	0.29	0.08
2381	3.86	35.95	10.53	10.65	4.52	0.08	0.49	0.20	12.41	7.43	7.65	0.65	0.01	4.34	0.28	0.01	0.37	0.50	0.07
2386	--	33.77	8.82	9.23	4.89	0.19	0.69	0.26	13.60	4.74	18.22	0.70	0.00	3.85	0.28	0.01	0.35	0.35	0.06
2387	0.68	36.57	9.79	10.81	4.66	0.12	0.52	0.23	12.44	4.89	13.16	2.29	0.02	2.85	0.24	0.01	0.36	0.28	0.08
2395	--	32.46	4.20	9.15	4.73	0.14	1.04	0.27	10.66	13.35	19.15	1.58	0.17	2.14	0.16	0.04	0.29	0.42	0.07
2396	1.18	37.33	4.46	10.22	5.08	0.57	0.87	1.33	10.99	4.35	17.48	2.39	0.06	2.66	0.18	0.01	0.33	0.40	0.09

Table 1 (continued)

Depth ¹	TOC	Quartz	K-feldspar	Plagioclase	Muscovite	Biotite	Kaolinite	Chlorite	Illite/ MLIS	Calcite	Dolomite	Fe- dolomite	Fe oxide and siderite	Pyrite	Sulphides ²	Fluorite	Ti silicates	Apatite	Heavy minerals
2401	0.48	37.15	4.46	10.98	6.54	0.95	0.98	1.62	16.05	3.76	10.93	0.96	0.02	3.83	0.51	0.01	0.36	0.36	0.05
2404	0.69	38.22	5.80	12.32	5.91	0.70	0.73	1.73	12.81	5.12	9.66	1.58	0.02	3.51	0.32	0.01	0.42	0.39	0.07
2408	--	39.14	5.76	12.08	3.99	0.50	0.66	1.62	9.22	7.81	11.30	4.40	0.07	2.49	0.14	0.02	0.42	0.33	0.06
2410	0.57	38.41	5.72	11.61	6.06	0.86	0.74	1.95	14.77	4.89	8.98	1.35	0.02	3.10	0.16	0.01	0.35	0.35	0.09
2414	--	41.86	6.35	10.75	4.91	0.73	0.65	1.65	14.57	5.56	7.20	1.58	0.02	3.20	0.16	0.01	0.37	0.35	0.07
2416	0.53	35.98	3.47	6.79	5.49	1.09	1.36	1.43	16.16	5.41	17.33	1.30	0.01	2.70	0.16	0.01	0.26	0.48	0.04
2425	1.06	44.59	6.12	12.13	3.69	0.46	0.60	1.71	13.41	5.91	5.34	0.80	0.02	3.23	0.19	0.01	0.36	0.32	0.06
2427	--	39.85	7.20	12.87	4.88	0.58	0.60	1.54	16.56	5.75	5.63	0.65	0.01	2.95	0.14	0.01	0.35	0.33	0.10
2431	0.83	41.20	6.35	11.41	4.89	0.73	0.69	1.54	14.41	4.25	9.63	0.88	0.00	2.32	0.10	0.01	0.39	0.27	0.09
2436	--	37.07	5.52	10.77	3.71	0.67	0.85	1.52	14.10	5.29	14.92	1.55	0.04	2.98	0.21	0.01	0.33	0.40	0.05
2440	0.87	32.32	3.10	5.36	3.40	0.86	1.29	1.07	19.84	2.98	21.37	1.21	0.00	5.58	0.24	0.01	0.23	0.24	0.03
2444	--	41.53	6.25	9.16	4.76	0.69	0.61	1.46	19.32	3.24	6.99	1.10	0.03	3.81	0.34	0.01	0.33	0.30	0.07
2448	1.60	41.20	6.05	9.23	4.62	0.75	0.72	1.44	20.13	2.90	6.05	0.70	0.02	3.67	0.22	0.01	0.36	0.26	0.08
2452	2.12	39.03	5.48	6.41	4.40	0.72	0.71	1.10	24.73	2.56	6.82	0.76	0.01	4.24	0.33	0.01	0.32	0.22	0.05
2457	--	33.14	3.57	7.49	3.24	0.65	0.99	1.50	15.15	3.50	22.46	4.67	0.09	2.80	0.19	0.01	0.30	0.20	0.05
2472	--	39.49	4.36	9.39	4.17	0.65	0.81	1.73	14.80	3.98	13.27	3.35	0.06	3.06	0.20	0.01	0.38	0.24	0.05
2474	1.35	38.97	4.30	7.11	2.63	0.87	0.49	1.05	25.75	4.80	6.67	1.40	0.03	3.67	0.23	0.00	0.40	0.24	0.04
2476	--	40.20	4.79	10.09	4.57	0.68	0.80	1.59	17.94	4.18	9.37	1.36	0.04	3.52	0.22	0.01	0.37	0.23	0.05
2479	1.38	35.10	3.58	7.18	2.50	0.88	0.68	1.19	23.11	5.32	11.11	3.59	0.03	3.47	0.20	0.00	0.40	0.23	0.05
2481	--	41.86	4.65	9.69	4.39	0.70	0.77	1.76	19.73	3.99	6.75	1.11	0.03	3.78	0.17	0.01	0.33	0.20	0.07
2483	0.97	41.39	4.44	8.30	4.05	0.65	0.74	1.39	20.29	3.94	7.61	1.11	0.05	4.17	0.28	0.01	0.32	0.23	0.06
2487	--	37.18	3.67	8.90	4.51	0.72	1.07	1.64	18.02	3.35	12.48	2.97	0.10	4.55	0.26	0.01	0.32	0.20	0.05
2492	0.97	40.76	4.14	9.04	4.70	0.76	0.89	1.56	19.68	4.00	7.63	0.98	0.04	4.07	0.20	0.01	0.35	0.20	0.04
2495	0.74	40.61	3.39	7.79	6.30	0.86	0.84	1.47	22.75	2.74	6.43	0.65	0.03	4.62	0.21	0.00	0.31	0.20	0.04
2498	--	26.33	1.67	4.08	2.90	0.78	1.83	1.36	12.79	2.27	34.74	7.47	0.27	3.03	0.10	0.01	0.19	0.15	0.03
2499	0.56	18.57	0.96	2.96	1.09	0.40	1.22	1.25	5.85	0.88	41.67	22.14	0.86	1.28	0.06	0.01	0.15	0.08	0.03
2501	0.96	43.60	3.85	7.81	5.11	0.80	0.74	1.45	22.95	3.49	4.70	0.61	0.03	3.23	0.13	0.01	0.32	0.15	0.07
2505	--	46.79	4.78	8.95	3.40	0.48	0.61	1.16	20.30	3.31	5.67	0.60	0.03	3.13	0.15	0.00	0.38	0.18	0.07
2509	1.40	45.39	4.21	6.95	3.23	0.41	0.66	0.98	19.73	3.27	7.79	1.24	0.07	3.83	0.20	0.01	0.38	0.18	0.05
2514	--	44.89	4.52	5.18	3.18	0.36	0.60	0.76	25.63	3.87	4.63	0.85	0.03	4.52	0.25	0.01	0.32	0.17	0.04
2518	2.10	38.93	3.79	3.97	1.89	0.28	0.74	0.55	27.24	5.75	8.44	1.45	0.01	4.23	0.20	0.01	0.24	0.14	0.04
2524	1.42	41.51	4.89	4.31	2.38	0.34	0.69	0.56	25.52	3.39	9.03	1.12	0.02	4.02	0.31	0.01	0.30	0.13	0.04
2528	--	44.95	5.30	4.42	3.41	0.25	0.44	0.47	29.23	1.31	4.39	0.23	0.01	4.45	0.66	0.00	0.29	0.14	0.05

¹Depths (in metres) in this table are shifted to match core gamma log with downhole gamma log.

²includes barite, sphalerite and gypsum.

Abbreviations: MLIS, mixed-layer illite-smectite; TOC, total organic carbon.

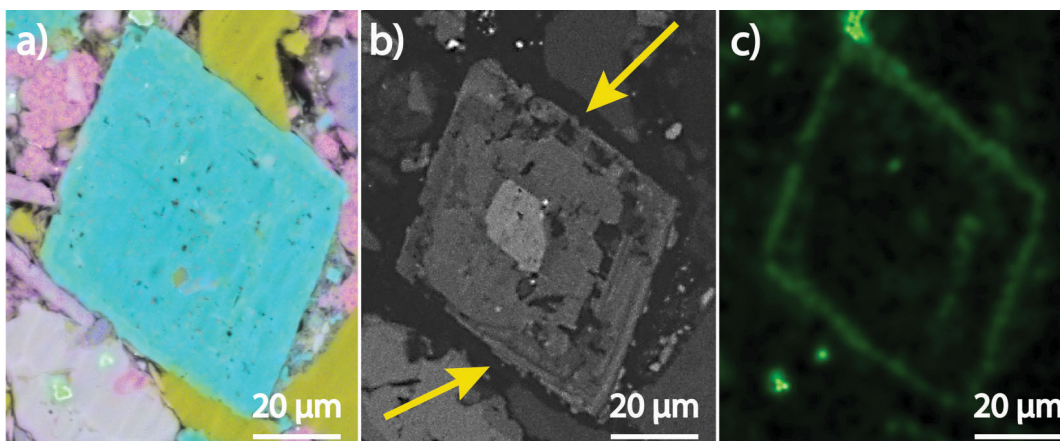


Figure 3. Dolomite cement in the Montney Formation, northeastern British Columbia. **a)** Energy dispersive spectrometry (EDS) image of dolomite (light blue). **b)** Scanning electron microscope (SEM) cathodoluminescence (CL) images of the crystals revealing complex internal structure with detrital rounded core and multiple rims. Some of the internal rims are corroded. Note the nonluminescent Fe-rich rim (yellow arrows). **c)** An EDS image showing Fe-rich external rim.

tions of dolomite cement were identified. Rims differ in Ca and Mg content (evidenced by HCl etching), with the outermost rim characterized by high Fe concentration (Figure 3). Several of the internal rims show corroded edges (Figure 3c). In some intervals, Ca-phosphate was incorporated into the dolomite structure. Dolomite dissolution is attributed to pressure solution (partially missing grain) or contact with organic acids (ragged edges; Figure 4a). Secondary porosity is developed in detrital dolomite, particularly along cleavage planes (Figure 4b).

Calcite

Calcite appears as isolated grains, sometimes enclosing large pyrite crystals (Figure 5a). The SEM-CL images show that calcite is composed of two generations (Figure 5b). Calcite was found to replace K-feldspar (Figure 5c) and dolomite (Figure 5d).

Ca-Phosphate (Apatite)

Ca-phosphate is present in the samples as grain-coating cement or nodules, and is locally incorporated into dolomite cement.

Pyrite

Pyrite is present in all samples, forming framboids or large crystals, and is commonly associated with organic matter. Framboids and crystals range from <1 to 10 µm in diameter (Figure 6).

K-Feldspar

Potassium-feldspar cement surrounds detrital K-feldspar grains as a one-phase cement (Figure 7a), or appears as discrete crystals with several generations of cement separated by dissolved ragged edges (Figure 7b). In addition, non-luminescent K-feldspar is detected in the centre of Na-feldspar and quartz grains (Figure 8). Most of the authigenic K-feldspar, though much darker than detrital K-feldspar in SEM-CL images, is moderately luminescent.

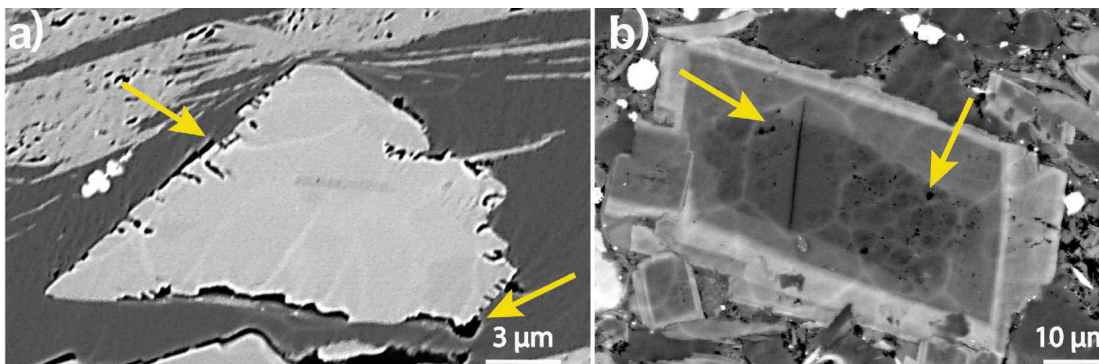


Figure 4. Backscattered electron–scanning electron microscope (BSE-SEM) images showing dolomite dissolution in the Montney Formation, northeastern British Columbia: **a)** dissolution of dolomite grain edges where dolomite is in direct contact with organic matter detrital grain and **b)** dissolution of detrital dolomite grain. Note preferred dissolution along cleavage planes.

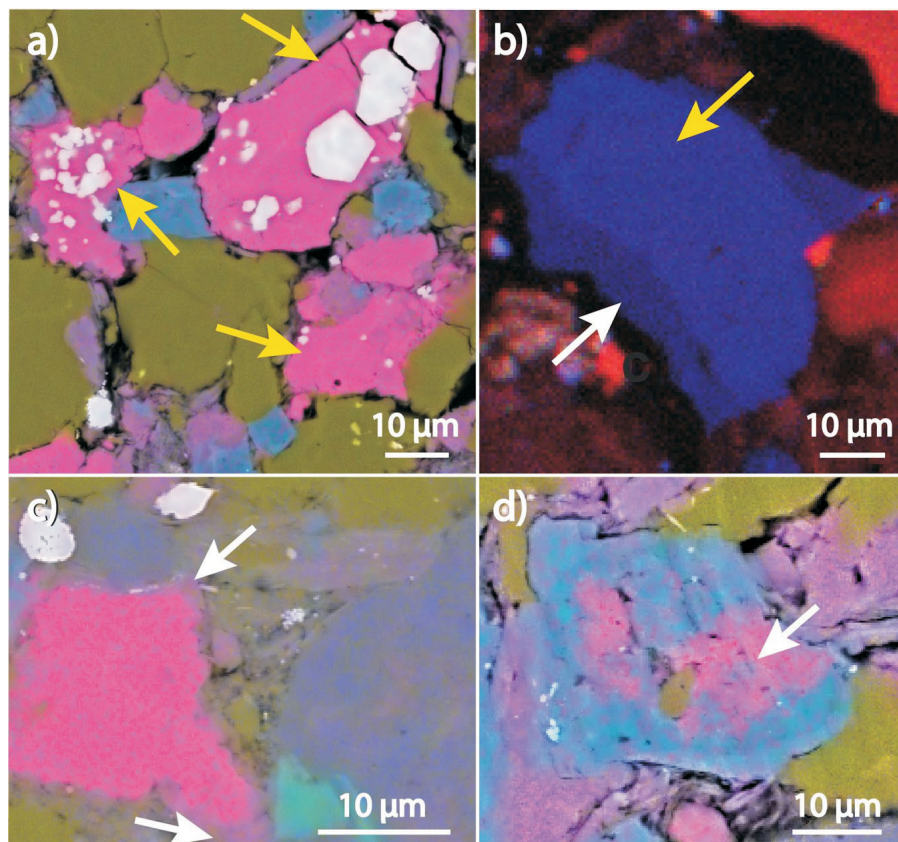


Figure 5. Scanning electron microscope images of calcite cement in the Montney Formation, northeastern British Columbia. **a)** Scanning electron microscope–energy dispersive spectrometry (SEM-EDS) image showing calcite (bright pink) enclosing pyrite crystals (white). **b)** Scanning electron microscope–cathodoluminescence (SEM-CL) image showing two different generations of calcite cement (different shades of blue) marked by arrows. **c)** An SEM-EDS image showing calcite (bright pink) replacing K-feldspar (light pink). In this image calcite has replaced most of the K-feldspar grain. Remaining K-feldspar is marked with arrows. **d)** An SEM-EDS image showing calcite replacing dolomite grain.

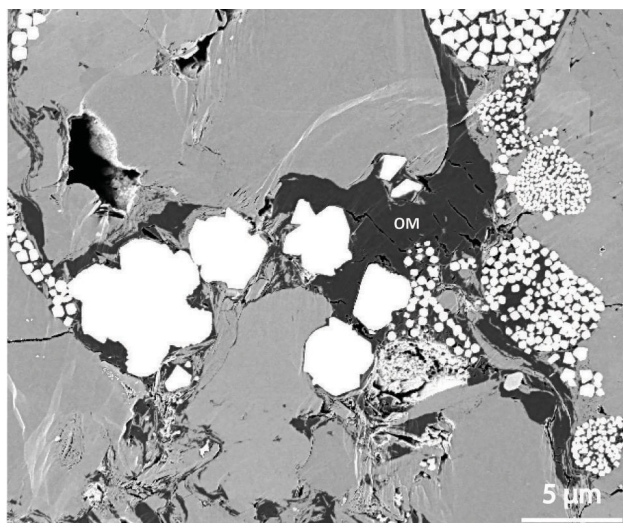


Figure 6. Backscattered electron–scanning electron microscope (BSE-SEM) image of a milled surface showing pyrite framboids and crystals (white) of varying sizes (Montney Formation, northeastern British Columbia). Note association with organic matter (OM, dark).

Na-Feldspar

In the deep Montney Formation, Na-feldspar largely occurs as detrital grains. Some samples contain nonluminescent Na-feldspar overgrowths with sharp, straight edges—both indicative of authigenic cement growth (Figure 9a). Nonluminescent Na-feldspar also replaces detrital and authigenic dolomite and detrital K-feldspar (Figure 9b, c). Sodium-feldspar alteration is usually incomplete and easily identifiable through EDS maps and backscattered electron (BSE)–SEM images.

Quartz

In the deep part of the Montney Formation, authigenic quartz occurs in three different morphologies: a) overgrowths, b) microcrystalline cements and c) amorphous opaline silica (Figure 10).

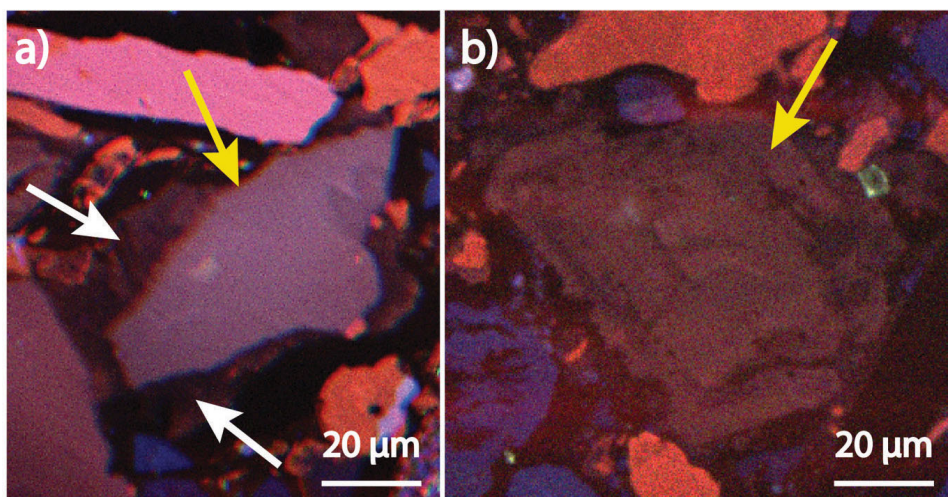


Figure 7. Scanning electron microscope–cathodoluminescence (SEM-CL) images of K-feldspar in the Montney Formation, northeastern British Columbia: **a)** detrital K-feldspar (yellow arrow) surrounded by K-feldspar cement (white arrows) and **b)** detrital rhombic K-feldspar showing cement rims (yellow arrow).

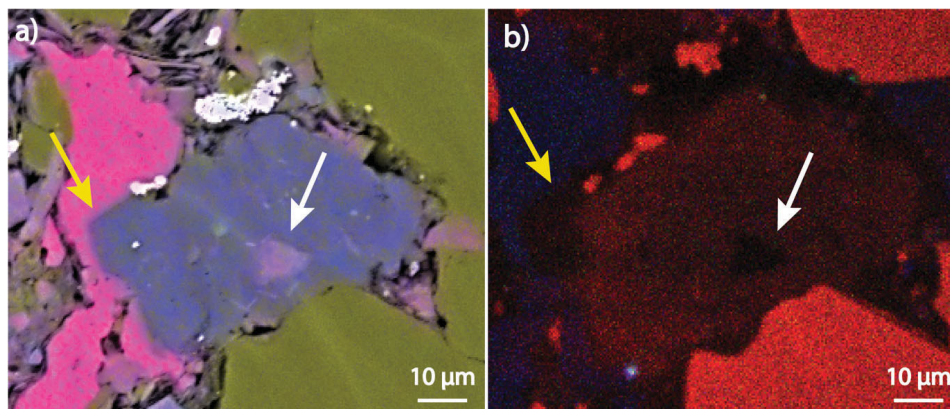


Figure 8. Sample from Montney Formation, northeastern British Columbia showing K-feldspar replacing Na-feldspar. **a)** Scanning electron microscope–energy dispersive spectrometry (SEM-EDS) image. Na-feldspar is represented by the blue colour and K-feldspar by the pink light colour and the white arrow. Yellow arrow points to straight edges of Na-feldspar cement. **b)** Scanning electron microscope–cathodoluminescence (SEM-CL) image. White arrow points to authigenic, nonluminescent K-feldspar. Note the straight edges of the Na-feldspar nonluminescent overgrowth (yellow arrow).

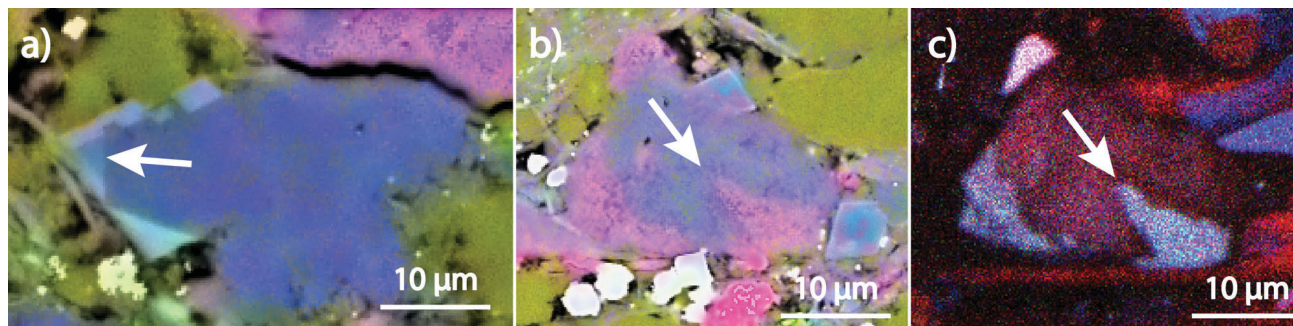


Figure 9. Examples of Na-feldspar replacement in the Montney Formation, northeastern British Columbia. **a)** Scanning electron microscope–energy dispersive spectrometry (SEM-EDS) image showing Na-feldspar (blue) replacing dolomite (light blue). Note two shades in the dolomite; the darker colour (white arrow) represents a detrital core and the lighter colour represents cement. **b)** An SEM-EDS image of Na-feldspar (blue) replacing detrital K-feldspar grain (pink). **c)** Scanning electron microscope–cathodoluminescence (SEM-CL) image of 9b. Note the bright colour of the K-feldspar (blue), indicating detrital origin.

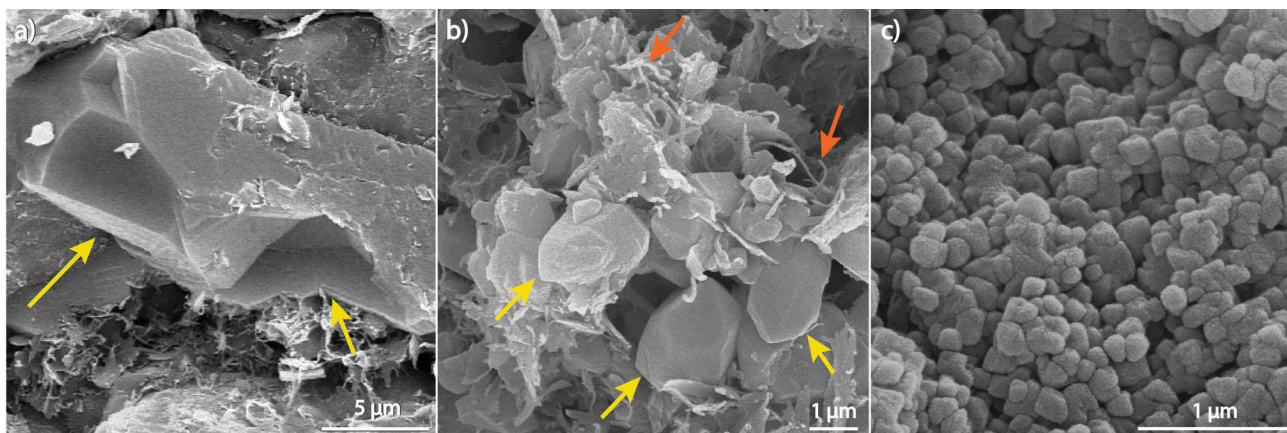


Figure 10. Secondary electron–scanning electron microscopy (SE-SEM) images of authigenic quartz morphologies in the deep Montney Formation, northeastern British Columbia: **a)** crystal overgrowth (arrows), note authigenic fibrous illite in the bottom section of the image; **b)** microcrystalline quartz cements (yellow arrows) and authigenic fibrous illite growing off the edges of detrital clay (orange arrow); and **c)** amorphous opaline silica.

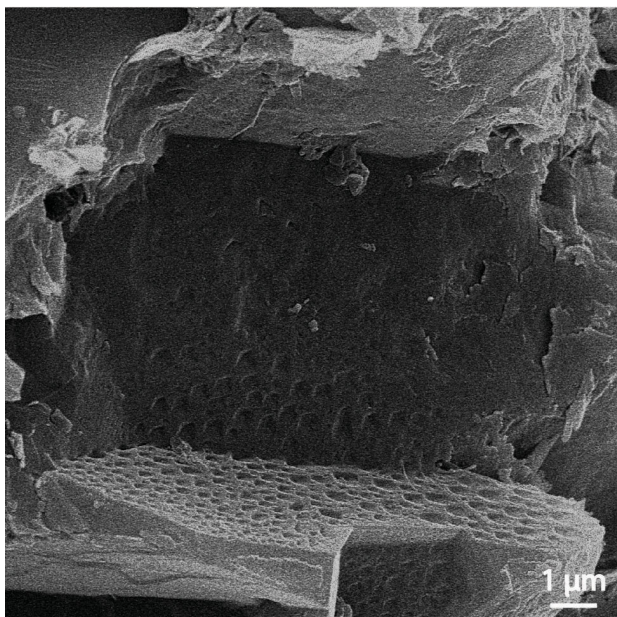


Figure 11. Secondary electron–scanning electron microscope (SE-SEM) image of a sample treated with HCl to remove carbonate. Angular small pits are visible on exposed quartz surfaces that were in contact with now dissolved carbonate cements. Pits are interpreted to be local quartz dissolution patterns. Sample from the Montney Formation, northeastern British Columbia.

Clay

Fibrous illite is present in the rock in varying abundance. Fibrous illite nucleates on the edges of detrital clay and locally on weathered mica grains (Figure 10b).

Porosity Enhancing Processes

Dolomite

Dolomite dissolution is evident by partially missing grains (Figure 2b) and ragged edges (Figure 4a). Secondary po-

rosity is developed in detrital dolomite, particularly along cleavage planes (Figure 4b).

Quartz

Small angular pits are present on the surface of some quartz grains (Figure 11). These pits are similar to previously reported quartz dissolution patterns (Freidman et al., 1976; Georgiev and Stoffers, 1980; Brantley et al., 1986; Burley and Kantorowicz, 1986; Hurst and Bjørkum, 1986; Bennett and Siegel, 1987; Knauss and Wolery, 1988; Wahab, 1998) and suggest local quartz dissolution in the Montney Formation caused by compaction.

Discussion

The Montney Formation in the study area is composed of compacted, well-cemented siltstone, containing detrital and authigenic phases, and organic matter. The QEM-SCAN results show that clay content in the deep Montney Formation ranges from 5 to 30 wt. %, with an average of 15 wt. %. These findings contrast with lower estimates of clay content previously published for the Montney Formation (<8 wt. %; Davies et al., 1997; Derder, 2012; Playter, 2013). Based on qualitative SEM observations most of the clay is of detrital origin.

The paragenesis of the Montney Formation in the deep basin was interpreted from a detailed study of crosscutting relationships between different phases. The paragenetic sequence is presented in Figure 12. In accord with other authors (Davies et al., 1997; Nassichuk, 2000; Barber, 2003; Chalmers and Bustin, 2012; Playter, 2013), the authors interpret dolomite as the earliest authigenic phase in the deep Montney Formation. Davies et al. (1997) analyzed fluid inclusions in the dolomite and concluded that dolomite was formed below 60°C. Dolomite precipitated in a series of rims, differing in composition (Ca/Mg), width and degree of corrosion on edges (Figure 3c). The outermost

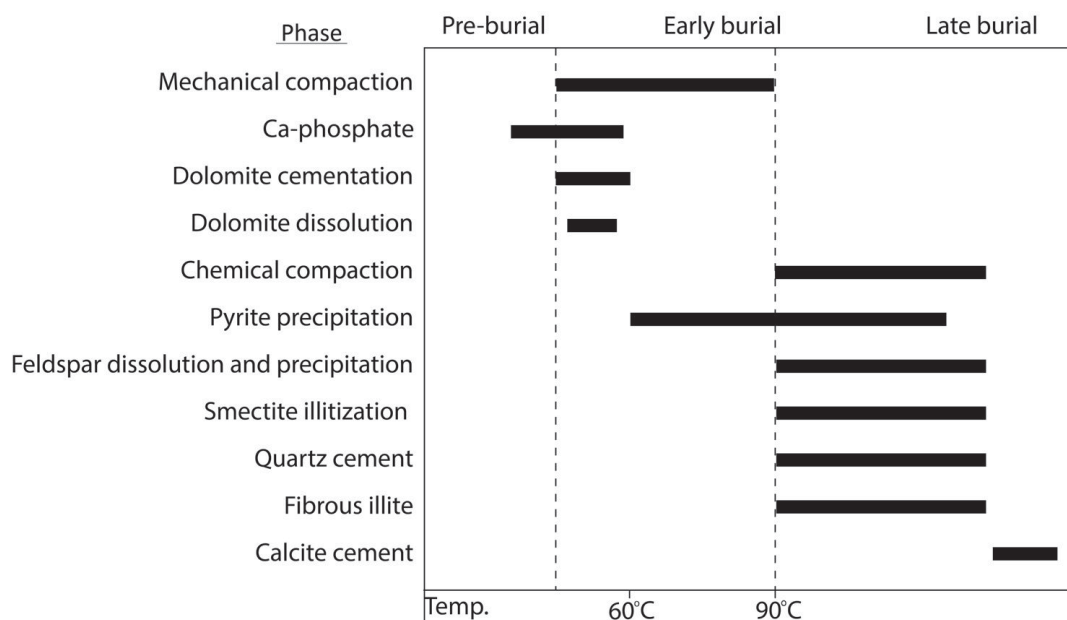


Figure 12. The paragenetic sequence for the Montney Formation in the deep basin, northeastern British Columbia.

Fe-rich rim of the dolomite is similar to that recognized by Davies et al. (1997) and Nassichuk (2000). Like Davies et al. (1997), the authors believe that Ca-phosphate precipitation is a syndepositional phase. Calcium phosphate, incorporated into dolomite cement, was probably remobilized during early burial (Tribovillard et al., 2006). Following dolomite precipitation, increasing burial led to chemical compaction and grain dissolution. The major phases that were dissolved are quartz, dolomite and feldspars. Since pyrite framboids and crystals are present in all cement phases in the Montney Formation (other than quartz, below), pyrite formation was interpreted to be a continuous diagenetic process.

The evolution of the feldspars in the deep Montney Formation is complicated and the temporal relationships between feldspar cementation and Na-feldspar to K-feldspar replacement remains unclear. The XRD analyses on glycolated samples resulted in 5% expandability of the MLIS, indicating extensive conversion of smectite to illite. In addition to smectite illitization, fibrous illite nucleated on detrital clay clumps or micas. Davies et al. (1997), Barber (2003) and Nassichuk (2000) described similar illitization processes as a result of K-feldspar dissolution.

The SEM imaging of freshly broken surfaces indicate relatively small authigenic quartz crystals (commonly <3 µm, occasionally up to 10 µm). Localized quartz dissolution is interpreted to occur during chemical compaction on contact surfaces between quartz and dolomite. Nassichuk (2000) reported that quartz partly or completely replaces dolomite, but this was not confirmed in this study. Playter (2013) proposed that dedolomitization occurred in the deep

Montney Formation, which was confirmed in this study (Figure 12), though not as a widespread phenomenon.

Future Work

This paper is part of a project that investigates the diagenesis of the Montney Formation. Future work will provide details on rock composition, diagenetic phases and the paragenetic sequence for the Montney Formation along a cross-section from the deep to shallow basin.

Conclusions

The Lower Triassic Montney Formation in the deep basin is composed of silt-size detrital and authigenic grains. Mixed-layer illite-smectite clay composes up to 30 wt. % of the rock. Diagenetic processes in the deep Montney Formation started with early burial and rock composition altered significantly over time. Dolomitization and feldspar alteration are the most volumetrically significant modifications. Both pore occluding and pore enhancing processes were observed, but porosity reduction processes are by far more substantial and significantly affect reservoir quality.

Acknowledgments

This work was supported by CMG Reservoir Simulation Foundation (Foundation CMG). The authors would like to thank M. Powers from SGS Canada Inc. for providing QEMSCAN® results and M. French for reviewing the manuscript. The authors would also like to warmly thank B. Jones for his comments and suggestions.

References

- Barber, L.M. (2003): Sedimentology, diagenesis and reservoir characterization of the Montney Formation at Sturgeon Lake South 'F' pool, west-central Alberta; M.Sc. thesis, University of Calgary, 557 p.
- BC Oil and Gas Commission (2016): Well lookup and reports; BC Oil and Gas Commission, web application, URL <<http://www.bcogc.ca/online-services>> [December 2016].
- Bennett, P. and Siegel, D.I. (1987): Increased solubility of quartz in water due to complexing by organic compounds; *Nature*, v. 326, p. 684–686.
- Brantley, S.L., Crane, S.R., Crerar, D.A., Hellmann, R. and Stallard, R. (1986): Dissolution at dislocation etch pits in quartz; *Geochimica et Cosmochimica Acta*, v. 50, p. 2349–2361.
- Burley, S.D. and Kantorowicz, J.D. (1986): Thin section and SEM textural criteria for the recognition of cement-dissolution porosity in sandstones; *Sedimentology*, v. 3, p. 587–604.
- Chalmers, G.R.L. and Bustin, R.M. (2012): Geological evaluation of Halfway-Doig-Montney hybrid gas shale-tight gas reservoir, northeastern British Columbia; *Marine and Petroleum Geology*, v. 38, p. 53–72.
- Crombez, V. (2016): Petrofacies, sedimentology and stratigraphic architecture of organic rich rocks. Insights from a multi-disciplinary study of the Montney and Doig formations (Lower and Middle Triassic, Alberta - British Columbia, Canada); Ph.D. thesis, Paris VI University, 238 p.
- Crombez, V., Baudin, F., Rohais, S., Riquier, L., Euzen, T., Pauthier, S., Mathieu, D., Caron, B. and Vaisblat, N. (2016): Basin scale distribution of organic matter in marine fine-grained sedimentary rocks: insight from sequence stratigraphy and multi-proxies analysis in the Montney and Doig formations; *Marine and Petroleum Geology*, in press, corrected proof, URL <<http://www.sciencedirect.com/science/article/pii/S0264817216303518>> [December 2016].
- Curtis, M.E., Ambrose, R.J., Sondergeld, C.H. and Rai, C.S. (2011): Transmission and scanning electron microscopy investigation of pore connectivity of gas shales on the nanoscale; Society of Petroleum Engineers, North American Unconventional Gas Conference and Exhibition, Woodlands, Texas, June 14–16, 2011, SPE-144391-MS, 10 p., URL <<https://www.onepetro.org/conference-paper/SPE-144391-MS>> [December 2016].
- Davies, G.R., Moslow, T.F. and Sherwin, M.D. (1997): The Lower Triassic Montney Formation, west-central Alberta; *Bulletin of Canadian Petroleum Geology*, v. 45, p. 474–505.
- Deep Times Maps Inc.TM (2013): North America 245 Ma Triassic (Early to Middle); Deep Times Maps Inc.TM, paleogeography map, URL <https://deeptimemaps.com/wp-content/uploads/2016/05/NAM_key-245Ma_ETri.png> [November 2016].
- Derder, O.M. (2012): Characterizing reservoir properties for the Lower Triassic Montney Formation based on petrophysical methods; M.Sc. thesis, University of Calgary, 231 p.
- Ducros, M., Euzen, T., Vially, R. and Sassi, W. (2014): 2-D basin modeling of the WCSB across the Montney-Doig system: implications for hydrocarbon migration pathways and unconventional resources potential; *in* Geoconvention 2014: Focus, Canadian Society of Petroleum Geologists, Canadian Society of Exploration Geophysicists, Canadian Well Logging Society, Joint Annual Meeting, Calgary, Alberta, May 12–14, 2014, abstract, 5 p. URL <http://www.geoconvention.com/archives/2014/185_GC2014_2D_basin_modeling_of_the_WCSB_across_the_Montney-Doig_system.pdf> [December 2016].
- Edwards, D.E., Barclay, J.E., Gibson, D.W., Kville, G.E. and Halton, E. (1994): Triassic Strata of the Western Canada Sedimentary Basin; *in* Geological Atlas of the Western Canada Sedimentary Basin, G.D. Mossop and I. Shetsen (comp.), Canadian Society of Petroleum Geologists, Calgary, Alberta and Alberta Research Council, Edmonton, Alberta, p. 259–275.
- Freidman, G.M., Ali, S.A. and Krinsley, D.H. (1976): Dissolution of quartz accompanying carbonate precipitation and cementation in reefs: example from the Red Sea; *Journal of Sedimentary Research*, v. 46, p. 970–973.
- Georgiev, V.M. and Stoffers, P. (1980): Surface textures of quartz grains from late Pleistocene to Holocene sediments of the Persian Gulf/ Gulf of Oman - an application of the scanning electron microscope; *Marine Geology*, v. 36, p. 85–96.
- Gibson, D.W. and Barclay, J.E. (1989): Middle Absaroka Sequence - the Triassic Stable Craton; *in* Western Canada Sedimentary Basin - A Case History, B.D. Ricketts (ed.), Canadian Society of Petroleum Geologists, Special Publication No. 30, p. 219–232.
- Golding, M.L., Orchard, M.J., Zonneveld, J.P. and Wilson, N.S.F. (2015): Determining the age and depositional model of the Doig Phosphate Zone in northeastern British Columbia using conodont biostratigraphy; *Bulletin of Canadian Petroleum Geology*, v. 63, p. 143–170.
- Golonka, J., Ross, M.I. and Scotese, C.R. (1994): Phanerozoic paleogeographic and paleoclimatic modeling maps; *in* Pangea: Global Environments and Resources, A.F. Embry, B. Beauchamp and D.J. Glass (ed.), Canadian Society of Petroleum Geologists, Memoir no. 17, p. 1–48.
- Hurst, A. and Bjørkum, P.A. (1986): Thin section and SEM textural criteria for the recognition of cement-dissolution porosity in sandstones; *Sedimentology*, v. 33, p. 605–614.
- Knauss, K.G. and Wolery, T.J. (1988): The dissolution kinetics of quartz as a function of pH and time at 70°C; *Geochimica et Cosmochimica Acta*, v. 52, p. 43–53.
- LaMothe, J.T. (2008): Sedimentology, ichnology, stratigraphy and depositional history of the contact between the Triassic Doig and Montney formations in west-central Alberta, Canada: presence of an unconformity bound sand wedge; M.Sc. thesis, University of Alberta, 184 p.
- Moslow, T.F. and Zonneveld, J.-P. (2012): The Montney Formation; unpublished industry course notes, Calgary, Alberta, May 29–31, 2012.
- Nassichuk, B.R. (2000): Sedimentology, diagenesis and reservoir development of the Lower Triassic Montney Formation, northeastern BC; M.Sc. thesis, University of British Columbia, 151 p.
- National Energy Board (2013): Canada's energy future 2013, energy supply and demand projections to 2035; National Energy Board, report, 87 p., URL <<https://www.neb-one.gc.ca/nrg/ntgrtd/fttr/2013/2013nrgftr-eng.pdf>> [November 2016].
- Playter, T.L. (2013): Petrographic and X-ray microtomographic analysis of the upper Montney Formation, northeastern British Columbia, Canada; M.Sc. thesis, University of Alberta, 111 p.

- Robbins, D.J.C. (1999): Ichnology and palaeoenvironment of the Lower Triassic Montney Formation, Kaybob and Kaybob South Fields area, west-central Alberta; M.Sc. thesis, University of Alberta, 165 p.
- Tribovillard, N., Algeo, T.J., Lyons, T. and Riboulleau, A. (2006): Trace metals as paleoredox and paleoproductivity proxies: an update; *Chemical Geology*, v. 232, p. 12–32.
- Vaisblat, N. and Harris, N.B. (2016): A burial history model for the Montney Formation - an insight to porosity distribution and hydrocarbon migration; *in* Geoconvention 2016: Optimizing Resources, Canadian Society of Petroleum Geologists, Canadian Society of Exploration Geophysicists, Canadian Well Logging Society, Joint Annual Meeting, Calgary, Alberta, March 7–11, 2016, abstract, 1 p., URL <http://www.geoconvention.com/uploads/2016abstracts/278_GC2016_A_Burial_History_Model_for_the_Montney_Fm.pdf> [December 2016].
- Wahab, A.A. (1998): Diagenetic history of Cambrian quartzarenites, Ras Dib-Zeit Bay area, Gulf of Suez, eastern desert, Egypt; *Sedimentary Geology*, v. 121, p. 121–140.
- Zonneveld, J.-P., Gingrass, K.M. and Beatty, T.W. (2010a): Diverse ichnofossil assemblages following the P-T mass extinction, Lower Triassic, Alberta and British Columbia, Canada: evidence for shallow marine refugia on the north-eastern coast of Pangea; *PALAIOS*, v. 25, p. 368–392.
- Zonneveld, J.-P., MacNaughton, R.B., Utting, J., Beatty, T.W., Pemberton, S.G. and Henderson, C.M. (2010b): Sedimentology and ichnology of the Lower Triassic Montney Formation in the Pedigree-Ring/Border-Kahntah River area, northwestern Alberta, and northeastern British Columbia; *Bulletin of Canadian Petroleum Geology*, v. 58, p. 115–140.
- Zonneveld, J.-P., Golding, M., Moslow, T.F., Orchard, M.J., Playter, T. and Wilson, N. (2011): Depositional framework of the Lower Triassic Montney Formation, west-central Alberta and northeastern British Columbia; *in* recovery 2011, Canadian Society of Petroleum Geologists, Canadian Society of Exploration Geophysicists, Canadian Well Logging Society, Joint Annual Meeting, Calgary, Alberta, May 9–13, 2011, abstract, 4 p.